

## BIVARIATE HAHN MOMENTS FOR IMAGE RECONSTRUCTION

HAIYONG WU<sup>\*,\*\*</sup>, SENLIN YAN<sup>\*\*</sup>

<sup>\*</sup> Lab of Image Science and Technology  
School of Computer Science and Engineering, Southeast University, 210096 Nanjing, China  
e-mail: enjoy3days@gmail.com

<sup>\*\*</sup> School of Mathematics and Information Technology  
Xiaozhuang University, 211171 Nanjing, China  
e-mail: senlinyan@163.com

This paper presents a new set of bivariate discrete orthogonal moments which are based on bivariate Hahn polynomials with non-separable basis. The polynomials are scaled to ensure numerical stability. Their computational aspects are discussed in detail. The principle of parameter selection is established by analyzing several plots of polynomials with different kinds of parameters. Appropriate parameters of binary images and a grayscale image are obtained through experimental results. The performance of the proposed moments in describing images is investigated through several image reconstruction experiments, including noisy and noise-free conditions. Comparisons with existing discrete orthogonal moments are also presented. The experimental results show that the proposed moments outperform slightly separable Hahn moments for higher orders.

**Keywords:** bivariate Hahn moments, bivariate Hahn polynomials, image reconstruction, pattern recognition.

### 1. Introduction

Moments and moment invariants have been widely used in image processing (Hu, 1962; Campisi *et al.*, 2004; Sroubek *et al.*, 2007; Žunić *et al.*, 2010; Papakostas *et al.*, 2010; Dai *et al.*, 2010; Fajarewicz, 2010). They can be divided into three categories: geometric moments, continuous orthogonal moments (Teague, 1980) and discrete orthogonal moments (Mukundan *et al.*, 2001; Yap *et al.*, 2003; 2007; Zhou *et al.*, 2005). Typical continuous orthogonal moments include Zernike moments and Legendre moments.

When one calculates continuous orthogonal moments for a digital image, it is necessary to discretize continuous integrals approximately and transform the image coordinate to the definition domain of Zernike and Legendre polynomials. These two steps lead to discretization errors and a higher time cost, respectively. Because discrete orthogonal polynomials such as Chebyshev, Krawtchouk and Hahn polynomials exactly satisfy the orthogonal property, they do not require any numerical approximation or spatial domain transformation (Mukundan *et al.*, 2001; See *et al.*, 2007). Hence, discrete orthogonal moments are proved to be

more suitable for image representation than continuous orthogonal moments.

For processing a two-dimensional image, a discrete orthogonal polynomial must be extended to two dimensions. There are two forms of two-dimensional polynomials, including a separable form and a non-separable form. Recently, Zhu (2012) has systematically addressed the theory of separable two-dimensional moments, whose basis functions are constructed by a tensor product of two different or same orthogonal polynomials in one variable, and several new types of continuous and discrete orthogonal moments have been proposed. Non-separable discrete orthogonal Charlier and Meixner moments are presented by Zhu *et al.* (2011).

Since the definition domains of Charlier and Meixner polynomials are  $[0, \infty]$ , they must be truncated to  $[0, N - 1]$  in defining moments of a digital image with size  $N \times N$ . This approximation leads to the result that the image representation capability of Charlier and Meixner moments is only comparable to Legendre moments, and is poorer than that of Chebyshev moments. However, the definition domain of Hahn

polynomials is exactly the same as that the image domain, while Meixner polynomials, Chebyshev polynomials and Krawtchouk polynomials are limit cases of Hahn polynomials, which encourages us to find more properties of Hahn polynomials. Dual Hahn polynomials are related to Hahn polynomials by switching the roles of  $x$  and  $n$  (in the definition of Hahn polynomials,  $x$  denotes the definition field and  $n$  denotes the order of polynomials), and the corresponding moments are proposed by Zhu *et al.* (2007). Unfortunately, dual Hahn polynomials are orthogonal on a non-uniform lattice, so an intermediate non-uniform lattice needs to be introduced before defining dual Hahn moments.

The purpose of this paper is to introduce a new kind of moments with bivariate Hahn polynomials as their basis function, and the proposed moments are expected to have a better image representation capability. The theory of multivariate orthogonal polynomials is an important topic of applied mathematics and physical applications. Continuous orthogonal polynomials of several variables have been long studied (Dunkl and Xu, 2001; Hunek, 2011). But discrete orthogonal polynomials have been less discussed due to their complicated structure. Xu (2004) identified discrete orthogonal polynomials of several variables in polynomial subspaces, and proved that they satisfied a three-term relation and Favard's theorem. He studied the second order partial difference equation of two variables to determine when it has orthogonal polynomials as solutions (Xu, 2005). Iliev and Xu (2007) found that second order difference equations have discrete orthogonal polynomials as their eigenfunctions. They provide a family of orthogonal basis explicitly, including Hahn polynomials of several variables. In the case of two dimensions, we call them *bivariate Hahn polynomials*. The computation of bivariate Hahn polynomials does not require a coordinate transformation and suitable approximation of the continuous moments integrals, which may lead further to high computational complexity and a discretization error. Taking them as the basic functions, we introduce a new set of *bivariate Hahn moments*, which are expected to hold a better image feature extraction capability compared with the existing discrete moments.

The remainder of this paper is organized as follows. In Section 2, we review the form of scaled Hahn polynomials of one variable, and briefly describe their computational algorithm. Then scaled bivariate Hahn polynomials are derived before the corresponding moments are defined. We illustrate the influence of parameter selection in detail. The reconstruction experiments for testing the performance of the proposed moments are shown in Section 3. They are compared with other existing discrete orthogonal moments. Finally, Section 4 concludes this paper.

## 2. Bivariate Hahn polynomials and moments

**2.1. Hahn polynomials of one variable.** Hahn polynomials of one variable  $x$ , with the order  $n$ , defined in the region of  $[0, N - 1]$  have the representation (Ismail *et al.*, 2008)

$$h_n(\alpha, \beta, N | x) = {}_3F_2 \left( \begin{matrix} -n, n + \alpha + \beta, -x \\ \alpha + 1, -N \end{matrix} \middle| 1 \right),$$

$$n, x = 0, 1, \dots, N - 1, \tag{1}$$

where  $\alpha, \beta$  are free parameters, and  ${}_3F_2(\cdot)$  is the generalized hyper-geometric function,

$${}_3F_2 \left( \begin{matrix} a_1, a_2, a_3 \\ b_1, b_2 \end{matrix} \middle| z \right) = \sum_{k=0}^{\infty} \frac{(a_1)_k (a_2)_k (a_3)_k}{(b_1)_k (b_2)_k k!} z^k, \tag{2}$$

while  $(a)_n$  is the Pochhammer symbol given by

$$(a)_n = a(a + 1) \dots (a + n - 1),$$

$$n \geq 1 \text{ and } (a)_0 = 1 \tag{3}$$

The Hahn polynomials satisfy the orthogonal property

$$\sum_{x=0}^{N-1} h_n(\alpha, \beta, N | x) h_m(\alpha, \beta, N | x) w(x) = \rho(n) \delta_{mn},$$

$$\tag{4}$$

where  $\delta_{mn}$  denotes the Kronecker symbol, and the weighting function  $w(x)$  is given by

$$w(x) = \frac{(\alpha + 1)_x (\beta + 1)_{N-x}}{(N - x)! x!}, \tag{5}$$

while  $\rho(n)$ , which is called the squared-norm, is expressed by

$$\rho(n) = \frac{(-1)^n n! (\beta + 1)_n (\alpha + \beta + n + 1)_{N+1}}{(-N)_n (2n + \alpha + \beta + 1) N! (\alpha + 1)_n}. \tag{6}$$

To overcome the shortcomings of numerical fluctuations, scaled Hahn polynomials are adopted frequently (Yap *et al.*, 2007),

$$\tilde{h}_n(\alpha, \beta, N | x) = h_n(\alpha, \beta, N | x) \sqrt{\frac{w(x)}{\rho(n)}}. \tag{7}$$

High order polynomials are usually deduced by the following recurrence relation with respect to  $n$ :

$$\tilde{h}_n(\alpha, \beta, N | x)$$

$$= A \sqrt{\frac{\rho(n-1)}{\rho(n)}} \tilde{h}_{n-1}(\alpha, \beta, N | x)$$

$$- B \sqrt{\frac{\rho(n-2)}{\rho(n)}} \tilde{h}_{n-2}(\alpha, \beta, N | x),$$

$$n = 2, 3, \dots, N - 1, \tag{8}$$

where

$$A = 1 + B - x \frac{(2n + \alpha + \beta + 1)(2n + \alpha + \beta + 2)}{(\alpha + \beta + n + 1)(\alpha + n + 1)(N - n)}, \quad (9)$$

$$B = \frac{n(n + \beta)(\alpha + \beta + n + N + 1)(2n + \alpha + \beta + 2)}{(2n + \alpha + \beta)(\alpha + \beta + n + 1)(\alpha + n + 1)(N - n)}. \quad (10)$$

The initial values for the above recursion can be obtained from

$$\tilde{h}_0(\alpha, \beta, N | x) = \sqrt{\frac{w(x)}{\rho(0)}}, \quad (11)$$

$$\tilde{h}_1(\alpha, \beta, N | x) = \left(1 - \frac{x(\alpha + \beta + 2)}{(\alpha + 1)N}\right) \sqrt{\frac{w(x)}{\rho(1)}}$$

or, equivalently, a recurrence relation with respect to  $x$  can be found in the work of Zhu *et al.* (2010).

Figure 1 shows the plots of several lower orders (orders of 0–4) of scaled Hahn polynomials of one variable. Polynomials with the parameters  $\alpha = \beta$  are shown in Figs. 1(a)–(d). They imply that the values of polynomials are symmetrically distributed about the center of the  $x$ -axis, and if the values of the parameters  $\alpha, \beta$  become larger, the distribution of polynomials will be concentrated in the intermediate definition domain of  $x$ . On the other hand, Figs. 1(e) and (f) show that the difference between the parameters  $\alpha$  and  $\beta$  will make the distribution of polynomials tend to one side of the definition of the domain. This property indicates that the Hahn moments can be utilized to extract local features just like Krawtchouk moments (Yap *et al.*, 2003).

Hahn moments of separable form have been first introduced by Zhou *et al.* (2005). Given an image with a density function  $f(x, y)$ , separable Hahn moments are defined as

$$HM_{mn} = \sum_{x=0}^{N-1} \sum_{y=0}^{N-1} \tilde{h}_m(\alpha, \beta, N | x) \tilde{h}_n(\alpha, \beta, N | y) f(x, y), \quad (12)$$

where  $N \times N$  is the size of the image. The orthogonality property of separable Hahn polynomials helps us in reconstructing the image using the following inverse transform:

$$f(x, y) = \sum_{m=0}^{N-1} \sum_{n=0}^{N-1} \tilde{h}_m(\alpha, \beta, N | x) \tilde{h}_n(\alpha, \beta, N | y) HM_{mn}. \quad (13)$$

In practical applications, the image can be approximately reconstructed from several low-order moments.

**2.2. Bivariate Hahn polynomials.** Bivariate Hahn polynomials defined on the domain with size  $N_1 \times N_2$  have the form (Iliev and Xu, 2007)

$$H_{n_1 n_2}(\eta, \gamma, N_1, N_2 | x_1, x_2) = (\eta + n_2 + 1)_{n_1} (\eta + x_1 + 1)_{n_2} \times h_{n_1}(\eta + n_2, n_2 + \gamma - 1, N_1 | x_1) \times h_{n_2}(\eta + x_1, N_1 - x_1 + \gamma - 1, N_2 | x_2), \quad (14)$$

where  $\eta$  and  $\gamma$  are free parameters, which means the values of  $\eta$  and  $\gamma$  do not affect the orthogonality of bivariate Hahn polynomials. Similarly, they satisfy the orthogonal property

$$\sum_{x_1=0}^{N_1-1} \sum_{x_2=0}^{N_2-1} H_{n_1 n_2}(\eta, \gamma, N_1, N_2 | x_1, x_2) \times H_{m_1 m_2}(\eta, \gamma, N_1, N_2 | x_1, x_2) w(x_1, x_2) = \rho(n_1, n_2) \delta_{n_1 m_1, n_2 m_2}, \quad (15)$$

where

$$w(x_1, x_2) = \frac{(-N_1)_{x_1} (-N_2)_{x_2}}{x_1! x_2!} \times \frac{(\eta + 1)_{(x_1+x_2)}}{(-N_1 - N_2 - \gamma + 1)_{(x_1+x_2)}}, \quad (16)$$

$$\rho(n_1, n_2) = \frac{(-1)^{(n_1+n_2)} (1 + \eta)_{(n_1+n_2)}}{(\gamma + n_1 + n_2)_{(N_1+N_2-n_1-n_2)}} \times \frac{n_1! (\eta + \gamma + 2n_2 + n_1)_{N_1+1}}{(-N_1)_{n_1} (\eta + \gamma + 2n_1 + 2n_2)} \times \frac{n_2! (\eta + \gamma + n_2 + N_1)_{N_2+1}}{(-N_2)_{n_2} (\eta + \gamma + 2n_2 + N_1)}. \quad (17)$$

Two non-separable Hahn polynomials of one variable serve as building blocks in Eqn. (14), which means they must be normalized before computing the corresponding bivariate polynomials. Substituting  $\alpha_1 = \eta + n_2, \beta_1 = n_2 + \gamma - 1$  and  $\alpha_2 = \eta + x_1, \beta_2 = N_1 - x_1 + \gamma - 1$  into Eqns. (5) and (6), we get

$$w_1(x_1) = \frac{(\eta + n_2 + 1)_{x_1} (n_2 + \gamma)_{N_1-x_1}}{(N_1 - x_1)! / x_1!}, \quad (18)$$

$$w_2(x_1, x_2) = \frac{(\eta + x_1 + 1)_{x_2} (N_1 - x_1 + \gamma)_{N_2-x_2}}{(N_2 - x_2)! / x_2!}, \quad (19)$$

$$\rho_1(n_1, n_2) = \frac{(-1)^{n_1} n_1! (n_2 + \gamma)_{n_1} (n_1 + 2n_2 + \eta + \gamma)_{N_1+1}}{(-N_1)_{n_1} (2n_1 + 2n_2 + \eta + \gamma)_{N_1} (n_2 + \eta + 1)_{n_1}} \quad (20)$$

$$\rho_2(n_1, n_2) = \frac{(-1)^{n_2} n_2! (\gamma - x_1 + N_1)_{n_2} (n_2 + \eta + \gamma + N_1)_{N_2+1}}{(-N_2)_{n_2} (2n_2 + \eta + \gamma + N_1)_{N_2} (\eta + x_1 + 1)_{n_2}} \quad (21)$$

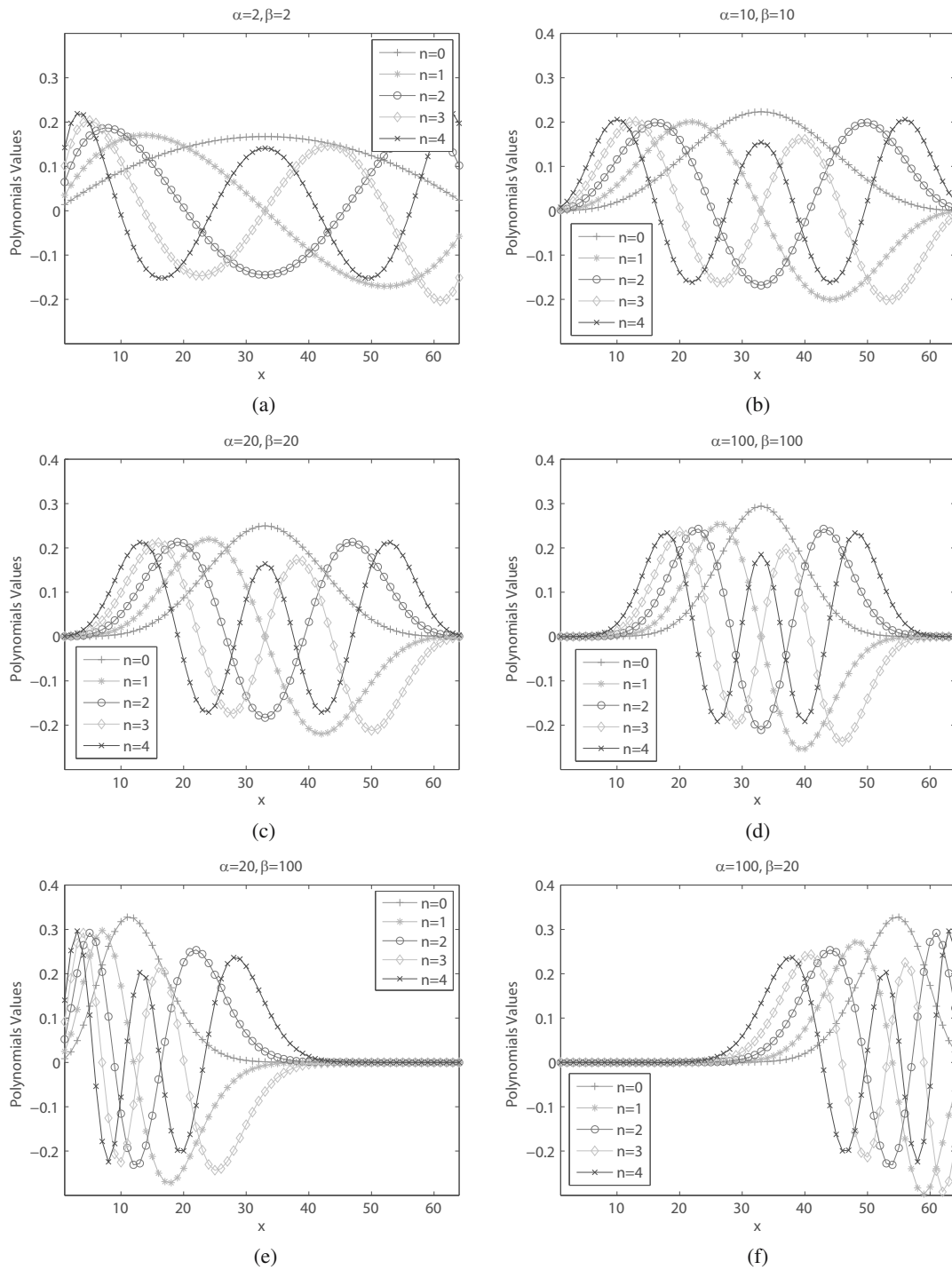


Fig. 1. Scaled discrete orthogonal Hahn polynomials of one variable ( $N = 64$ ).

After tedious manipulation, we can obtain

$$\frac{((\eta + n_2 + 1)_{n_1}(\eta + x_1 + 1)_{n_2})^2 w(x_1, x_2)}{\rho(n_1, n_2)} = \frac{w_1(x_1)w_2(x_1, x_2)}{\rho_1(n_1, n_2)\rho_2(n_1, n_2)}. \quad (22)$$

Therefore,

$$\begin{aligned} & \tilde{H}_{n_1 n_2}(\eta, \gamma, N_1, N_2 | x_1, x_2) \\ &= \sqrt{\frac{w(x_1, x_2)}{\rho(n_1, n_2)}} H_{n_1 n_2}(\eta, \gamma, N_1, N_2 | x_1, x_2) \\ &= \tilde{h}_{n_1}(\eta + n_2, n_2 + \gamma - 1, N_1 | x_1) \\ & \quad \times \tilde{h}_{n_2}(\eta + x_1, N_1 - x_1 + \gamma - 1, N_2 | x_2) \end{aligned} \quad (23)$$

and

$$\sum_{x_1=0}^{N_1-1} \sum_{x_2=0}^{N_2-1} \tilde{H}_{n_1 n_2}(\eta, \gamma, N_1, N_2 | x_1, x_2) \quad (24)$$

$$\tilde{H}_{m_1 m_2}(\eta, \gamma, N_1, N_2 | x_1, x_2) = \delta_{n_1 m_1, n_2 m_2}.$$

**2.3. Influence of parameters  $\eta, \gamma$ .** Since the parameters  $\eta$  and  $\gamma$  have no distinct meaning in the definition of bivariate Hahn polynomials, we study them using a number of plots. In the first example, we consider the case  $\eta = \gamma$ . Parameters varying from small to large are tested: (a)  $\eta = \gamma = 1$ , (b)  $\eta = \gamma = 5$ , (c)  $\eta = \gamma = 10$ , (d)  $\eta = \gamma = 15$ , (e)  $\eta = \gamma = 20$ , (f)  $\eta = \gamma = 25$ . Figure 2 depicts the first order of bivariate Hahn polynomials ( $N = 64$ ) with the same parameters. It implies that the polynomials contract to the centre as parameters increase. Moreover, the values of the polynomials are symmetric along both the dimensions. These conclusions are identical to those of scaled Hahn polynomials of one variable.

In the second experiment, we consider the case  $\eta \neq \gamma$ . Parameter  $\gamma$  is assigned a constant value of 10, which is a middle value between 1 and 20. Let the parameter  $\eta$  change: (a)  $\eta = 1$ , (b)  $\eta = 5$ , (c)  $\eta = 15$ , (d)  $\eta = 20$ , i.e., two cases are greater than  $\gamma$  and two cases are less than  $\gamma$ . The first order of bivariate Hahn polynomials ( $N = 64$ ) is plotted in Fig. 3. We can observe that the values of bivariate Hahn polynomials move from the left to the right of the  $x_2$  axis as  $\eta$  increases. The values are not symmetrical about the center of the definition domain. Generally, information of an image is evenly distributed in the central region of the image. Hence, bivariate Hahn moments with different parameters are not suitable to extract global features of an image. We only take the case  $\eta = \gamma$  into account in consecutive experiments.

**2.4. Bivariate Hahn moments.** Given an  $N \times N$  image  $f(x_1, x_2)$ , its bivariate Hahn moment of  $(n_1 + n_2)$  order is defined as

$$M_{n_1, n_2} = \sum_{x_1=0}^{N-1} \sum_{x_2=0}^{N-1} \tilde{H}_{n_1, n_2}(\eta, \gamma, N, N | x_1, x_2) f(x_1, x_2). \quad (25)$$

According to Eqn. (24), we can obtain the corresponding inverse transform,

$$f(x_1, x_2) = \sum_{n_1=0}^{N-1} \sum_{n_2=0}^{N-1} \tilde{H}_{n_1, n_2}(\eta, \gamma, N, N | x_1, x_2) M_{n_1, n_2}. \quad (26)$$

Due to the orthogonal property of the kernel functions, Eqn. (26) implies that each moment makes an independent contribution to the reconstructed image. If the moments are limited to an order  $P$ , Eqn. (26) is approximated by

$$\hat{f}(x_1, x_2) = \sum_{n_1=0}^{P-1} \sum_{n_2=0}^{P-1} \tilde{H}_{n_1, n_2}(\eta, \gamma, N, N | x_1, x_2) M_{n_1, n_2}. \quad (27)$$

### 3. Experimental results

To validate the feature representation capability of the proposed moments, we invoke them to achieve image reconstruction. A reconstructed image can be obtained according to Eqn. (27). Different evaluation criteria are applied to measure the performance of binary and grayscale image reconstructions. In this section, reconstructions are applied to a set of binary images and two sets of grayscale images. The experimental results are compared with other discrete orthogonal moments in both noise-free and noisy conditions.

**3.1. Appropriate choice of parameters  $\eta$  and  $\gamma$ .** In the previous section, we conclude that the parameters  $\eta = \gamma$  are suitable to extract global features of an image. It is necessary to determinate appropriate values of parameters  $\eta$  and  $\gamma$  before image reconstruction experiments. Set A consists of 100 binary images selected from the MPEG-7 CE-2 database (Zhang and Lu, 2001). Set B is composed of 100 color images chosen from the COIL100 database (Nene *et al.*, 1988), and 100 color images chosen from the WBIIS database (Wang *et al.*, 1997) form set C. The color images in sets B and C are converted to the grayscale format. Then, images of the three sets are resized to  $64 \times 64$  before experiments. Figure 4 shows six samples from the three sets. Two different color sets are used since their distributions of pixel intensities are significantly different: images in set B are centered, while images in set C are global.

In order to measure the performance of the reconstruction, we adopt an objective measure, a reconstruction error, for a reconstruction of a binary image (Yap *et al.*, 2003),

$$\varepsilon = \frac{1}{N^2} \sum_{x=0}^{N-1} \sum_{y=0}^{N-1} |f(x, y) - T(\hat{f}(x, y))|, \quad (28)$$

where  $f(x_1, x_2)$  is the original image pixel intensity at  $(x_1, x_2)$ , and  $\hat{f}(x_1, x_2)$  is its reconstructed version. The operator  $T(\cdot)$  is defined by

$$T(z) = \begin{cases} 1 & \text{if } z \geq 0.5, \\ 0 & \text{if } z < 0.5. \end{cases} \quad (29)$$



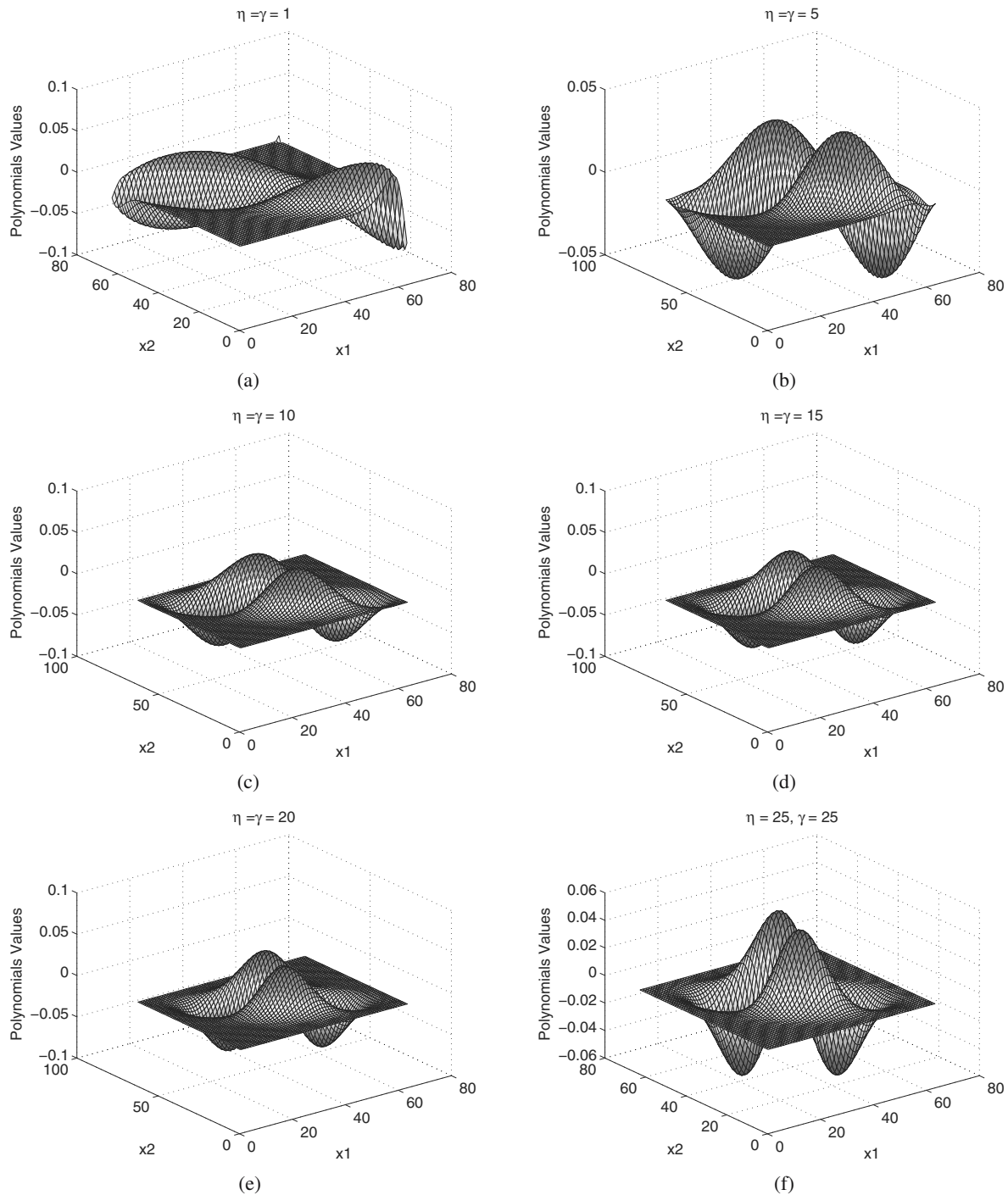


Fig. 2. First order of bivariate Hahn polynomials ( $N = 64$ ) with the equivalent parameters.

For gray images, however, neither Eqn. (28) nor the MSE (Mean Squared Error) is suitable for predicting human perception of image fidelity and quality. The Structural Similarity Index Measure (SSIM) is utilized frequently instead of the MSE in many perceptual comparisons (Wang *et al.*, 2004). In practice, one usually requires a single overall quality measure of the entire image. We use a Mean SSIM (MSSIM) index to evaluate

the overall quality of a reconstructed image (Wang and Bovik, 2009).

Reconstructions are repeated with different parameters through the three tested databases. The reconstruction order is up to 50. Figure 5(a) depicts the average reconstruction error of set A, and Fig. 5(b) shows a reconstruction result of Fig. 4(a) as a sample. We can observe from Figs. 5(a) and (b) that reconstruction

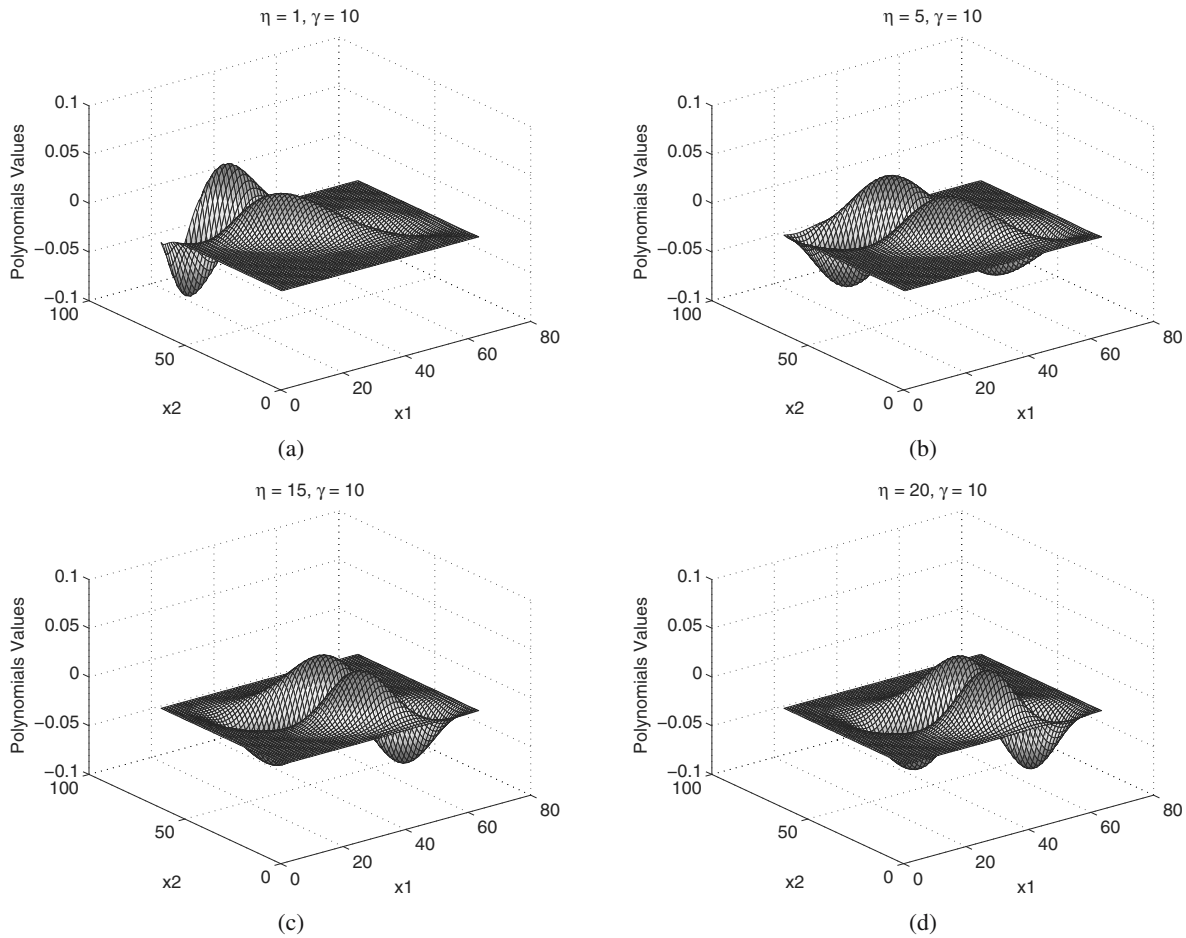


Fig. 3. First order of bivariate Hahn polynomials ( $N = 64$ ) with different parameters.

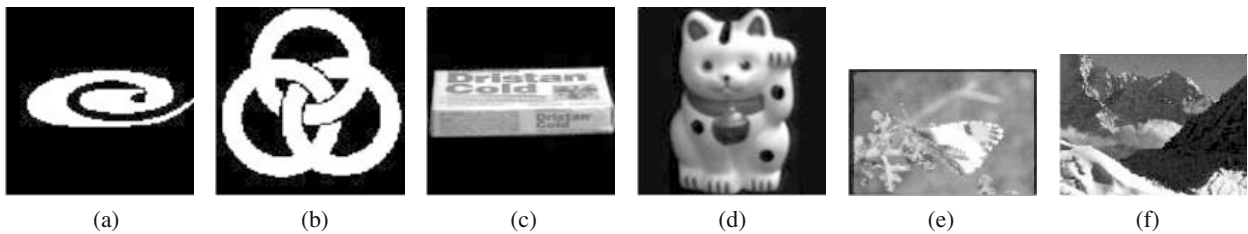


Fig. 4. Sample images: (a) and (b) are from MPEG-7 CE-2, (c) and (d) are from COIL100, (d) and (e) are from WBIIS.

errors decrease as parameters  $\eta$  and  $\gamma$  increase. When the parameters are greater than 25, there is little difference. We think this is because binary images of set A (see Figs. 4(a) and (b)) contain little information on four sides, and bivariate Hahn polynomials are approximately concentrated in the middle of the region of definition as the parameters increase (see Fig. 2). Figures 5(c) and (e) show the average MSSIM index of sets B and C, respectively. Reconstruction results of Figs. 4(d) and (f) are shown in Figs. 5(d) and (f), respectively. Figures 5(c)–(f) suggest that we should choose larger values for  $\eta$  and  $\gamma$  without considering the density distribution of the image. Unlike the MSE, the MSSIM

index emphasizes structural details, so moments with larger parameters can provide a higher structural similarity. Therefore, we can set parameters  $\eta = \gamma = 25$  in the following experiments.

**3.2. Comparisons against other discrete moments.**

Comparisons begin with reconstructions of binary images. Images in set A are utilized to compare the performance among Chebyshev moments, separable Hahn moments and bivariate Hahn moments. It should be noted that all parameters of separable Hahn moments are set to 20 ( $\alpha_1 = \beta_2 = \alpha_2 = \beta_1 = 20$ ) (Zhou *et al.*, 2005). The averages reconstruction error and a sample reconstruction

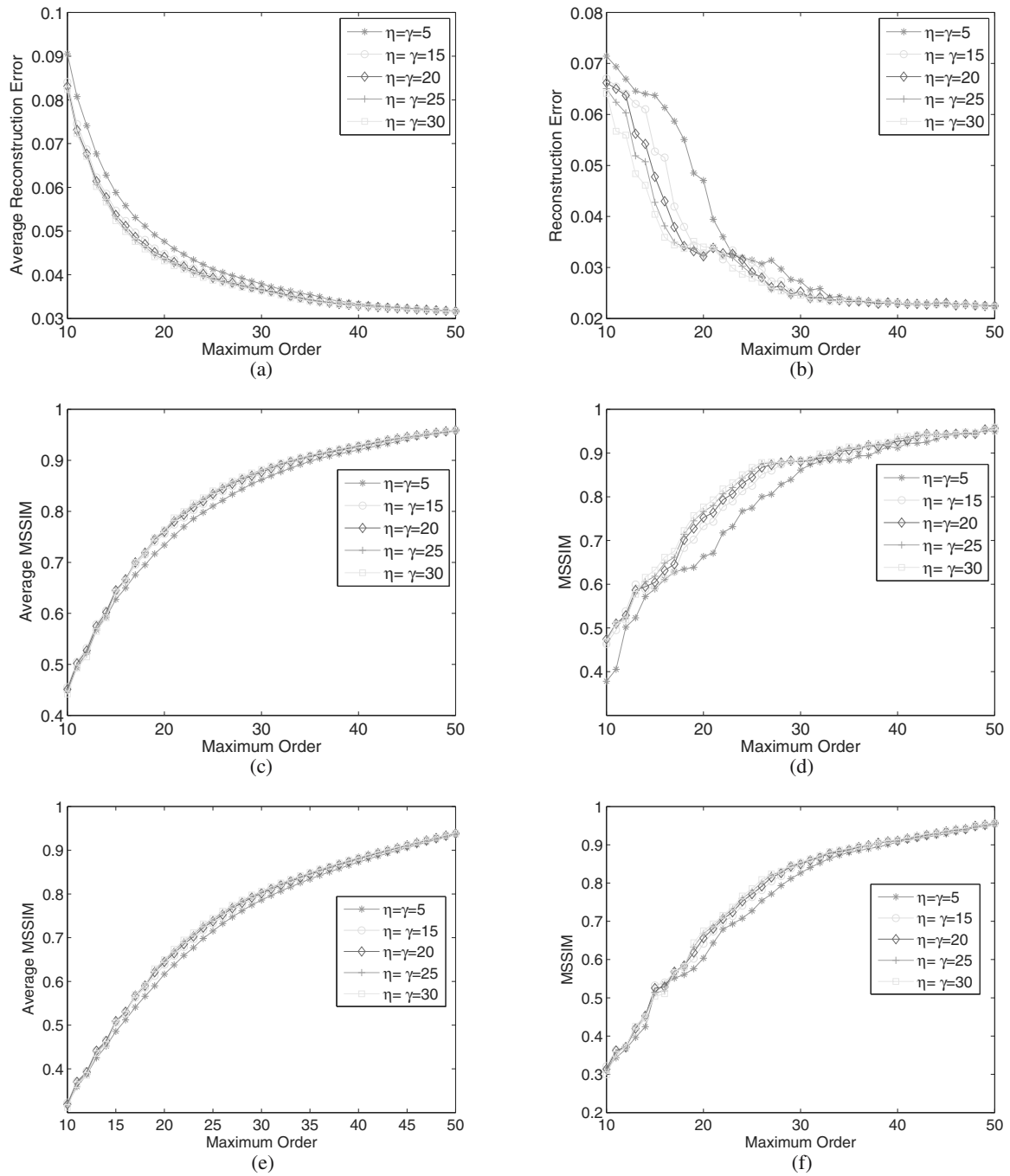


Fig. 5. Reconstruction results with different parameters.

comparison of Fig. 4(a) are shown in Figs. 6(a) and (b), respectively. We can observe that both separable and bivariate Hahn moments outperform Chebyshev moments, and the proposed descriptor has a slightly better performance than separable Hahn moments, when the reconstruction order is greater than 20.

This is because the emphasis of bivariate Hahn moments, with  $\eta = \gamma = 25$ , approximately focuses on the center of the image.

The grayscale images obtained from sets B and C are applied to compare the performance of the proposed moments against the other discrete orthogonal moments. Figures 7(a) and (c) show the average MSSIM of sets B and C, respectively. Figures 7(b) and (d) show MSSIM index of two samples given in Figs. 4(d) and (f), respectively. Conclusions achieved from Fig. 7 are identical to those drawn from Fig. 6. Moreover, the overall performance of the MSSIM index of set B is better than



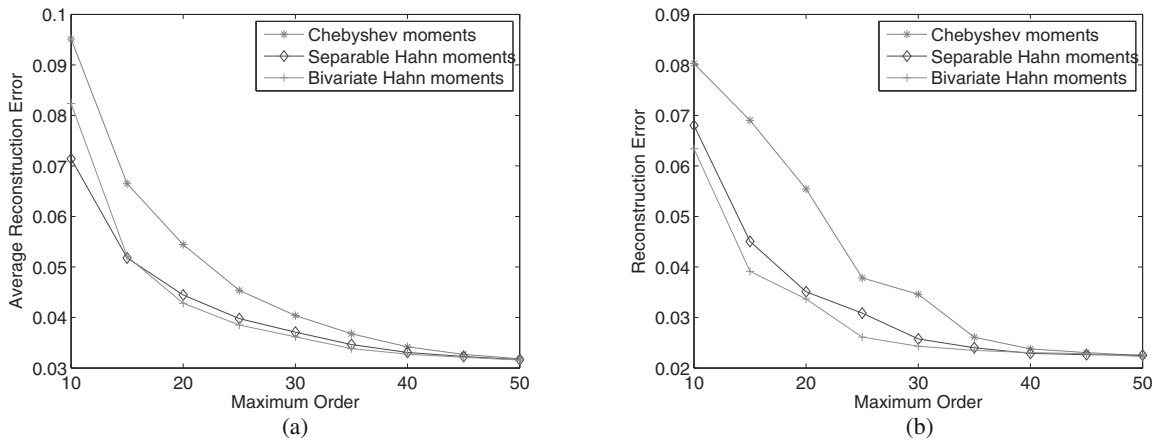


Fig. 6. Reconstruction errors of a binary image.

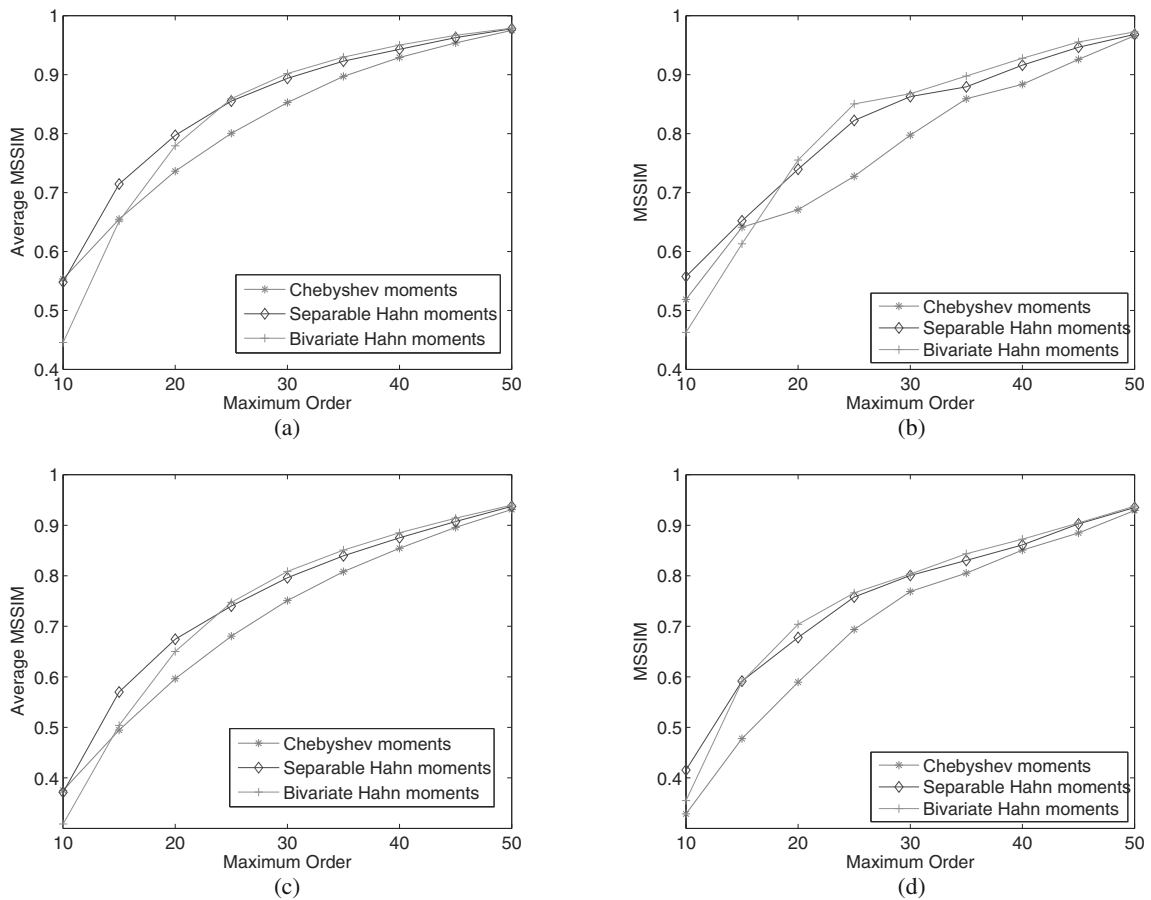


Fig. 7. MSSIM index comparisons of reconstruction for grayscale images.

that of set C. This is because bivariate Hahn moments with large parameters can extract more central details of an image.

**3.3. Robustness to noise.** Sensitivity to noise is usually considered a critical indicator for image moments. Three testing sets are corrupted by difference additive noises: set A is degraded by salt-and-pepper noise with

density 0.05 and 0.1, sets B and C are corrupted by Gaussian noise with zero mean and variance  $\sigma^2 = 0.01$  and 0.03. The overall performance comparisons of the three sets are depicted in Figs. 8(a)–(f).

Two standard images and the corresponding degraded versions are shown in the first row of Fig. 9. They are invoked in reconstruction procedures repeatedly. Reconstructed images using different moments are

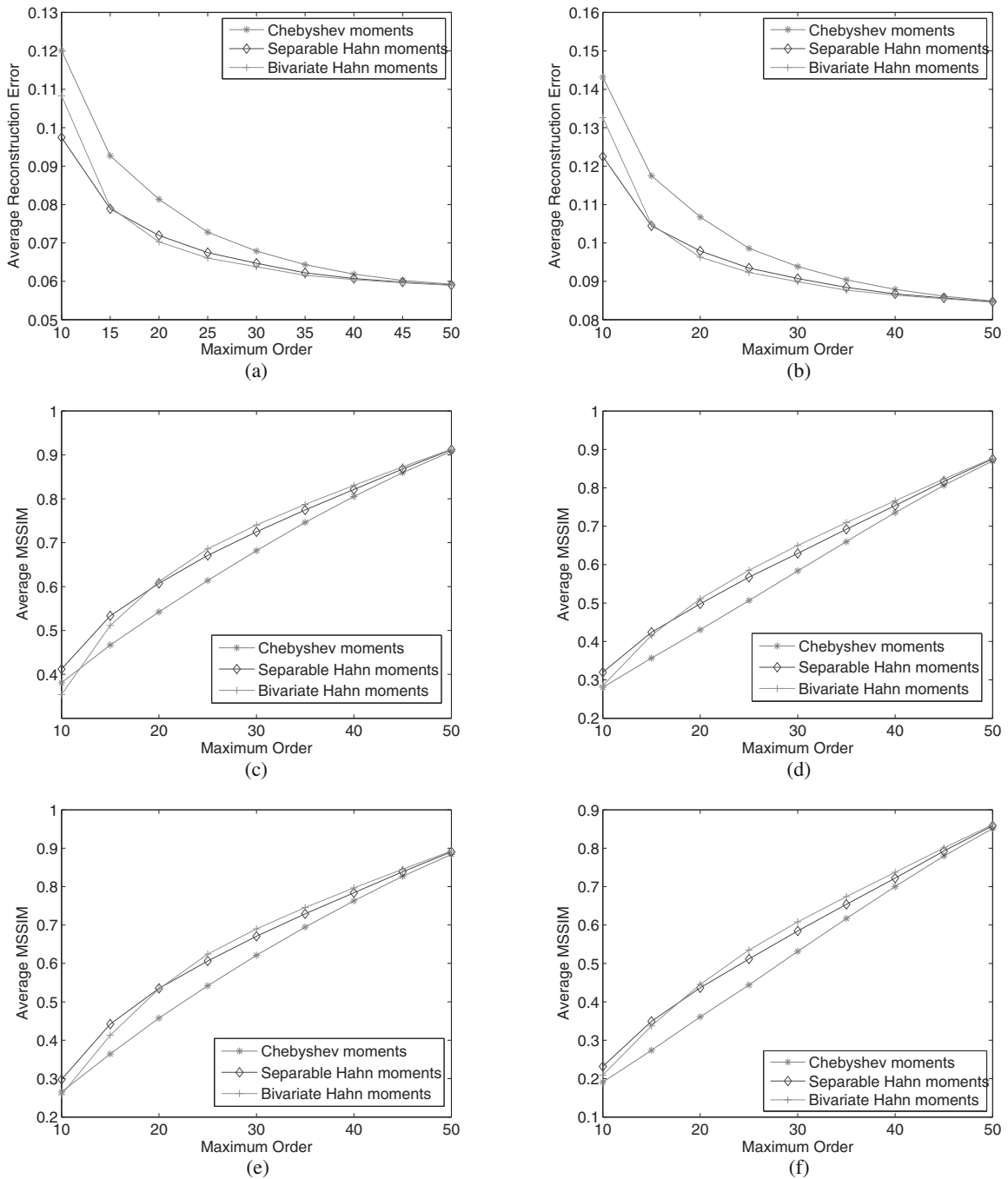


Fig. 8. Overall performance comparisons of robustness to noise: average reconstruction errors of set A (a), average MSSIM index of set B (b), average MSSIM index of set C (c).

depicted in the bottom rows of Fig. 9. Compared with existing orthogonal moments, our proposed moments exhibit more robustness to different noise signals.

#### 4. Conclusion

This paper introduces a new set of bivariate Hahn moments with a non-separable orthogonal basis for

describing image features. The normalization of bivariate Hahn polynomials and selection of parameters were discussed in detail. Reconstruction experiments were carried out to verify their image representation capability. The results were compared with other existing orthogonal discrete moments such as Chebyshev and traditional separable Hahn moments. Images with and without noise were utilized to evaluate the performance

original binary image	degraded by salt and pepper noise with density 0.05	degraded by salt and pepper noise with density 0.1	original gray-scale image	degraded by Gaussian noise with $\mu=0$ and $\sigma=0.01$	degraded by Gaussian noise with $\mu=0$ and $\sigma=0.03$
$\varepsilon = 0.0017$	$\varepsilon = 0.0080$	$\varepsilon = 0.0229$	MSSIM=0.9623	MSSIM=0.8322	MSSIM=0.7688
Reconstructed images using Chebyshev moments					
$\varepsilon = 0.0005$	$\varepsilon = 0.0071$	$\varepsilon = 0.0190$	MSSIM=0.9631	MSSIM=0.8354	MSSIM=0.7729
Reconstructed images using separate Hahn moments					
$\varepsilon = 0.0005$	$\varepsilon = 0.0059$	$\varepsilon = 0.0188$	MSSIM=0.9681	MSSIM=0.8369	MSSIM=0.7784
Reconstructed images using bivariate Hahn moments					

Fig. 9. Reconstructed images with orders up to 50.

of the proposed moments.

The reconstructed images and detailed error showed that bivariate Hahn moments outperform slightly with the increase in the order. Moreover, our proposed moments have fewer parameters to be determined, which may imply that they are more suitable for practical applications.

However, due to the bivariate form of polynomials, the values of moments cannot be achieved by the method presented by Yap *et al.* (2003). The values of bivariate Hahn moments are obtained only via pixel-by-pixel computations, and this process is very time consuming. Thus, our future work will focus on the fast algorithm to determine bivariate Hahn polynomials and corresponding moments.

### Acknowledgment

This work was supported by the Natural Science Foundation of Xiaozhuang University (No. 2009NXY12). We would like to thank the anonymous reviewers for their constructive comments and suggestions to improve the quality of this paper.

### References

- Campisi, P., Neri, A., Panci, G. and Scarano, G. (2004). Robust rotation-invariant texture classification using a model based approach, *IEEE Transactions on Image Processing* **13**(6): 782–791.
- Dai, X., Shu, H., Luo, L., Han, G.N. and Coatrieux, J.L. (2010). Reconstruction of tomographic images from limited range projections using discrete Radon transform and Tchebichef moments, *Pattern Recognition* **43**(3): 1152–1164.
- Dunkl, C.F. and Xu, Y. (2001). *Orthogonal Polynomials of Several Variables*, Cambridge University Press, Cambridge.
- Fujarewicz, K. (2010). Planning identification experiments for cell signaling pathways: An NF $\kappa$ B case study, *International Journal of Applied Mathematics and Computer Science* **20**(4): 773–780, DOI: 10.2478/v10006-010-0059-6.
- Hu, M. (1962). Visual pattern recognition by moment invariants, *IRE Transactions on Information Theory* **8**(2): 179–187.
- Iliev, P. and Xu, Y. (2007). Discrete orthogonal polynomials and difference equations of several variables, *Advances in Mathematics* **212**(1): 1–36.
- Ismail, M., Foncannon, J. and Pekonen, O. (2008). Classical and quantum orthogonal polynomials in one variable, *The Mathematical Intelligencer* **30**(1): 54–60.

- Mukundan, R., Ong, S. and Lee, P.A. (2001). Image analysis by Tchebichef moments, *IEEE Transactions on Image Processing* **10**(9): 1357–1364.
- Nene, S., Nayar, S. and Murase, H. (1988). *Columbia Object Image Library (coil 100) 1996*, Ph.D. thesis, Columbia University, New York, NY.
- Papakostas, G., Karakasis, E. and Koulouriotis, D. (2010). Novel moment invariants for improved classification performance in computer vision applications, *Pattern Recognition* **43**(1): 58–68.
- See, K., Loke, K., Lee, P. and Loe, K. (2007). Image reconstruction using various discrete orthogonal polynomials in comparison with DCT, *Applied Mathematics and Computation* **193**(2): 346–359.
- Sroubek, F., Cristóbal, G. and Flusser, J. (2007). A unified approach to superresolution and multichannel blind deconvolution, *IEEE Transactions on Image Processing* **16**(9): 2322–2332.
- Teague, M.R. (1980). Image analysis via the general theory of moments, *Journal of the Optical Society of America A* **70**(8): 920–930.
- Wang, J.Z., Wiederhold, G., Firschein, O. and Wei, S.X. (1997). Wavelet-based image indexing techniques with partial sketch retrieval capability, *Proceedings of the IEEE International Forum on Research and Technology Advances in Digital Libraries, ADL 1997, Washington, DC, USA*, pp. 13–24.
- Wang, Z. and Bovik, A.C. (2009). Mean squared error: Love it or leave it? A new look at signal fidelity measures, *IEEE Signal Processing Magazine* **26**(1): 98–117.
- Wang, Z., Bovik, A.C., Sheikh, H.R. and Simoncelli, E.P. (2004). Image quality assessment: From error visibility to structural similarity, *IEEE Transactions on Image Processing* **13**(4): 600–612.
- Hunek, W.P. and Latawiec, K.J. (2011). A study on new right/left inverses of nonsquare polynomial matrices, *International Journal of Applied Mathematics and Computer Science* **21**(2): 331–348, DOI: 10.2478/v10006-011-0025-y.
- Xu, Y. (2004). On discrete orthogonal polynomials of several variables, *Advances in Applied Mathematics* **33**(3): 615–632.
- Xu, Y. (2005). Second-order difference equations and discrete orthogonal polynomials of two variables, *International Mathematics Research Notices* **2005**(8): 449–475.
- Yap, P.T., Paramesran, R. and Ong, S.H. (2003). Image analysis by Krawtchouk moments, *IEEE Transactions on Image Processing* **12**(11): 1367–1377.
- Yap, P. T., Paramesran, R. and Ong, S. H. (2007). Image analysis using Hahn moments, *IEEE Transactions on Pattern Analysis and Machine Intelligence* **29**(11): 2057–2062.
- Zhang, D. and Lu, G. (2001). Content-based shape retrieval using different shape descriptors: A comparative study, *Proceedings of the International Conference on Intelligent Multimedia and Distance Education, ICIMADE01, Fargo, ND, USA*, pp. 1–9.
- Zhou, J., Shu, H., Zhu, H., Toumoulin, C. and Luo, L. (2005). Image analysis by discrete orthogonal Hahn moments, in J.S. Marques, N. Pérez de la Blanca and P. Pina (Eds.), *Image Analysis and Recognition*, Springer, Berlin/Heidelberg, pp. 524–531.
- Zhu, H. (2012). Image representation using separable two-dimensional continuous and discrete orthogonal moments, *Pattern Recognition* **45**(4): 1540–1558.
- Zhu, H., Liu, M., Li, Y., Shu, H. and Zhang, H. (2011). Image description with nonseparable two-dimensional Charlier and Meixner moments, *International Journal of Pattern Recognition and Artificial Intelligence* **25**(1): 37–55.
- Zhu, H., Liu, M., Shu, H., Zhang, H. and Luo, L. (2010). General form for obtaining discrete orthogonal moments, *IET Image Processing* **4**(5): 335–352.
- Zhu, H., Shu, H., Zhou, J., Luo, L. and Coatrieux, J.L. (2007). Image analysis by discrete orthogonal dual Hahn moments, *Pattern Recognition Letters* **28**(13): 1688–1704.
- Žunić, J., Hirota, K. and Rosin, P.L. (2010). A Hu moment invariant as a shape circularity measure, *Pattern Recognition* **43**(1): 47–57.



**Haiyong Wu** was born in 1976. He received the B.Sc. degree in physics from Jiangsu Normal University in 1997, the M.Sc. degree in electronic engineering from the Nanjing University of Aeronautics and Astronautics in 2003, and is currently pursuing the Ph.D. degree at the School of Computer Science, Southeast University, Nanjing, China. He is also an associate professor in the School of Mathematics and Information Technology, Nanjing Xiaozhuang University. His research interests include pattern recognition and image processing.



**Senlin Yan** was born in 1962. He received the B.Sc. (1983) and M.Sc. (1995) degrees in physics from Nanjing Normal University and Jiangxi Normal University, respectively, and the Ph.D. degree in electronics and engineering from Southeast University in 2001. Now, he is a professor in the School of Mathematics and Information Technology, Nanjing Xiaozhuang University. His research interest includes optical communication, optical computation and nonlinear optics and lasers.

Received: 1 May 2013

Revised: 9 November 2013

Re-revised: 13 December 2013